

Europium as a lodestar: diagnosis of radiogenic heat production in terrestrial exoplanets

Spectroscopic determination of Eu abundances in α Centauri AB \star

H. S. Wang¹, T. Morel², S. P. Quanz¹, and S. J. Mojzsis^{3,4}

¹ Institute for Particle Physics and Astrophysics, ETH Zürich, Wolfgang-Pauli-Strasse 27, 8093 Zürich, Switzerland
e-mail: haiwang@phys.ethz.ch; sascha.quanz@phys.ethz.ch

² Space sciences, Technologies and Astrophysics Research (STAR) Institute, Université de Liège, Quartier Agora, Allée du 6 Août 19c, Bât. B5C, B4000-Liège, Belgium
e-mail: tmorel@uliege.be

³ Department of Geological Sciences, University of Colorado, UCB 399, 2200 Colorado Avenue, Boulder, CO 80309-0399, USA
e-mail: stephen.mojzsis@colorado.edu

⁴ Institute for Geological and Geochemical Research, Research Centre for Astronomy and Earth Sciences, Hungarian Academy of Sciences, H-1112 Budapest, Hungary

Received 09 May 2020 / Accepted xxx

ABSTRACT

Context. Long-lived radioactive nuclides, such as ^{40}K , ^{232}Th , ^{235}U and ^{238}U , contribute to persistent heat production in the mantle of terrestrial-type planets. As refractory elements, the concentrations of Th and U in a terrestrial exoplanet are implicitly reflected in the photospheric abundances in the stellar host. However, a robust determination of these stellar abundances is difficult in practice owing to the general paucity and weakness of the relevant spectral features.

Aims. We draw attention to the refractory, *r*-process element europium, which may be used as a convenient and practical proxy for the population analysis of radiogenic heating in exoplanetary systems.

Methods. As a case study, we present a determination of Eu abundances in the photospheres of α Cen A and B with high-resolution HARPS spectra and a strict line-by-line differential analysis. To first order, the measured Eu abundances can be converted to the abundances of ^{232}Th , ^{235}U and ^{238}U with observational constraints while the abundance of ^{40}K is approximated independently with a Galactic chemical evolution model.

Results. Our determination shows that europium is depleted with respect to iron by ~ 0.1 dex and to silicon by ~ 0.15 dex compared to solar in both binary components. The loci of α Cen AB at the low-ends of both [Eu/Fe] and [Eu/Si] distributions of a large sample of FGK stars further suggest significantly lower potential of radiogenic heat production in any putative terrestrial-like planet (i.e. α -Cen-Earth) in this system, compared to that in rocky planets (including our own Earth) formed around the majority of these Sun-like stars. Based on our calculations of the radionuclide concentrations in the mantle and assuming the mantle mass to be the same as that of our Earth, we find that the radiogenic heat budget in an α -Cen-Earth is $73.4^{+8.3}_{-6.9}$ TW upon its formation and $8.8^{+1.7}_{-1.3}$ TW at the present day, respectively 23 \pm 5% and 54 \pm 5% lower than that in the Hadean Earth (94.9 ± 5.5 TW) and in the modern Earth (19.0 ± 1.1 TW).

Conclusions. As a consequence, mantle convection in an α -Cen-Earth is expected to be overall weaker than that of Earth (assuming other conditions are the same) and thus such a planet would be less geologically active, suppressing its long-term potential to recycle its crust and volatiles. With Eu abundances being available for a large sample of Sun-like stars, the proposed approach can extend our ability to make predictions about the nature of other rocky worlds that can be tested by future observations.

Key words. Stars: abundances – Stars: individual (α Cen A, α Cen B) – Planets and satellites: composition

1. Introduction

A major goal of modern astronomy is to better define the nature of exoplanets and understand planet formation and evolution, as well as life prospects, in a cosmic perspective. To this end, communities in Earth sciences, exoplanet science, and stellar astrophysics have been increasingly joining forces, through existing and future, ground- and space-based astronomical infrastructures (e.g. Gaia, VLT, Kepler, TESS, ELT, JWST, PLATO) and/or collaboration networks (e.g. NExSS, PlanetS, GALAH).

Through spectroscopic observations of their photospheres, one can decipher the elemental compositions of stars, which in

turn yield unique insights into the formation and bulk compositions of the planets formed around them (Bond et al. 2010; Pagano 2014; Wang et al. 2019a; Doyle et al. 2019; Liu et al. 2020). The resulting data can be used to infer gross geodynamical properties (including interior, surface, atmosphere, as well as habitability) of terrestrial-like exoplanets (Frank et al. 2014; Noack et al. 2017; Hinkel & Unterborn 2018; Wang et al. 2019b; Shahar et al. 2019).

Radiogenic heat generated by the decay of the long-lived radionuclides (^{40}K , ^{232}Th , ^{235}U and ^{238}U) contributes a time-dependent but significant proportion of the Earth's internal heat (e.g. Gando et al. 2011; Lenardic et al. 2011; Frank et al. 2014;

\star Based on observations collected at the La Silla Observatory, ESO (Chile) with the HARPS spectrograph.

Nimmo 2015)¹, which powers mantle convection leading to persistent plate tectonics, plume activity and other forms of volcanism that eventually made our planet habitable (Sleep 2007; Lugaro et al. 2018; Lingam & Loeb 2020; Seales & Lenardic 2020). Therefore, knowing the abundances of these long-lived, heat-producing isotopes in other rocky planets is critical to the assessment (to first order) of the geological activity of these planets.

The other main source of planetary internal heat is the dynamical/gravitational energy, inherited from planet formation and core-mantle segregation; this declines with time² owing to secular cooling (Stevenson 2003; Lyubetskaya & Korenaga 2007). An expression of the relative importance between radio-genic heating and the gravitational energy is dubbed the Urey ratio/number, which is defined as the ratio of the instantaneous radiogenic heat production to the total surface heat flow of the planet at that time; proposed values range from approximately 0.3 to 0.9 for the case of the Earth (Schubert et al. 2001)³. Yet, placing direct constraints on the Urey number for exoplanets is not possible due to the paucity of information related to the multitude of possible disc environments, planet formation histories and evolution scenarios. With these important caveats, it makes sense to start with the host stellar abundances to make preliminary inferences about rocky worlds around other stars (Santos et al. 2017; Doyle et al. 2019; Wang et al. 2019b; Liu et al. 2020) that can be verified (or refuted) as new observational techniques come online.

On top of this, challenges also exist in spectroscopically determining the abundances of the principal long-lived radioactive elements in planet-hosting stars (e.g. Unterborn et al. 2015; del Peloso et al. 2005; Botelho et al. 2019).⁴ As a result, selecting other elements that can act as proxies and are easier to measure is a convenient and practical approach, especially for population analysis of potential rocky worlds around other stars.

Owing to the fact that U and Th are pure neutron-capture (rapid-) *r*-process elements (Simmerer et al. 2004; Bisterzo et al. 2014), the surrogates should also be produced through this nucleosynthesis channel as much as possible. Based on this criterion, Ir and Eu – 98.4 and 94.0% contributions by *r*-process, respectively (Bisterzo et al. 2014) – are most suitable proxy candidates for U and Th. Because the Eu abundances are considerably easier to determine in extrasolar systems, we regard it as the appropriate choice here (as supported by Yong et al. 2008). There are also other proxies for long-lived radionuclides discussed in the literature, e.g., Hf, Bi and Tl (Sneden et al. 2008; Wilford 2011). However, Eu must clearly be preferred given the large sets of Eu abundances for FGK dwarfs (e.g. Pagano 2014; Delgado Mena et al. 2017; Battistini & Bensby 2016; Mishenina

et al. 2016; Guiglion et al. 2018), which overwhelmingly exceed what is available for other proxy candidates (see, e.g., Hinkel et al. 2019). The abundance measurements of the latter proxies are either restricted to stars with very peculiar chemical patterns (e.g. Roederer et al. 2018) or not possible at all, as illustrated by the absence of their lines in the solar photospheric spectrum (e.g. Bi and Tl; Grevesse et al. 2015). In addition, because of the high *r*-process contribution to Eu, it has been used extensively together with a typical *s*-process element (e.g. Ba) as a chemical clock in nucleosynthesis as well as to assess the *r*-process enrichment in galaxy chemical evolution histories (Mashonkina & Gehren 2000; Jacobson & Friel 2013; Ji et al. 2016; Bisterzo et al. 2016; Skúladóttir et al. 2019).

Observations of both Eu and Th abundances in solar analogues with a wide range of ages (0-10 Ga) have shown that the [Eu/H] and initial [Th/H] abundance ratios evolve in lockstep: [Th/Eu] is solar within 0.04 dex during the Galactic thin disk evolution (Botelho et al. 2019). Measurements in meteoritic and in Galactic halo stars have also shown a nearly constant U/Th production ratio ($0.571^{+0.037}_{-0.031}$; Dauphas 2005). In addition, Eu is a refractory element (with a condensation temperature even slightly higher than Fe and Ni; see Lodders 2003 and Wood et al. 2019), which implies that its abundance in a terrestrial planet is representative and closely related to that of the stellar host. Finally, Eu has stable isotopes and an age correction is thus not necessary to estimate its pristine abundance at the time of planet formation. However, we must note in advance that ^{40}K cannot be directly/indirectly informed from Eu due to its distinct nucleosynthesis pathways (Clayton 2003; Zhang et al. 2006) as well as its volatile nature (Wang et al. 2019a). Instead, alternative assumptions (detailed below) have to be made regarding ^{40}K .

The recognition that Eu is a suitable reference element for long-lived radionuclides (excluding ^{40}K) is by no means new (Pagel 1989), but one can argue that its usefulness as a proxy for (partial) internal heat production has not been fully recognised by the exoplanet community (e.g. Kite et al. 2009). The vast majority of stars potentially hosting terrestrial-like planets actually do not have Eu abundances available (e.g. Schuler et al. 2015). As demonstrated in the following, Eu abundances can be spectroscopically determined with relative ease even in stars that are not necessarily (very) bright, thanks to the moderate strength of the Eu II lines in the blue spectral range. Therefore, it is also hoped that our study will motivate more widespread determinations of the abundance of this element in stars with potentially rocky planets.

As a case study, we turn our attention to our nearest Sun-like star systems, α Cen AB, at only \sim 1.3 pc. Although no planet orbiting either binary component has been confirmed yet (e.g. Dumusque et al. 2012; Hatzes 2013; Rajpaul et al. 2016), various numerical simulations support the contention that the stability of planetary orbits can persist within the so-called habitable zones of these two binary stars (Andrade-Ines & Michtchenko 2014; Quarles & Lissauer 2016, 2018). If a small (potentially rocky) planet is discovered in the habitable zone of either α Cen A or B, the intensive discussion about the nature of such a planet would be brought to the forefront. The detailed chemical composition of α Cen AB recently revisited by Morel (2018, hereafter M18) enables such a discussion to be made *quantitatively*, except for the planetary internal heat budget partially owing to the lack of abundances of heat-producing elements (U, Th, and K) or their proxies. In the context of exoplanet studies and, in particular, our modelling of the radiogenic heat power in the putative planets orbiting α Cen A or B, we present in this work our spectroscopic analysis and results of Eu abundances of both stars (Sects. 2 and

¹ The heat-producing short-lived nuclides ^{26}Al and ^{60}Fe are important heating sources in shaping the composition of planetesimals in the early solar system (Lichtenberg et al. 2016) but become effectively extinct after 3 Myrs and essentially have no contribution to heat production in already formed planets (Frank et al. 2014).

² Radiogenic heating also declines with time but in different ways, i.e. following the exponent decay of radionuclides.

³ Another similar concept is called "the convective Urey ratio" (Korenaga 2008), which refers to the mantle contribution alone. However, we do not distinguish it from the (total) Urey number we have adopted here since that would require the crustal information, which is far from being ascertained with our current observations of exoplanets.

⁴ For instance, the Th abundance is commonly determined through modelling of a single line (Th II λ 4019.1) that is heavily blended with stronger features of other elements (e.g. Fe and Ni) and very sensitive to continuum placement.

3), followed by a comparison with previous Eu analyses for α Cen A/B (Sect. 4.1) and with Eu abundances of other stars (Sect. 4.2). We provide an assessment of radiogenic heat budget for potential, terrestrial planets in the system (Sect. 4.3), together with an analysis of the limitations to our approach (Sect. 4.4). Our conclusions are summarised in Sect. 5.

2. Analysis

Aiming for a homogeneous spectroscopic analysis of the Eu abundances in α Cen AB, we closely follow the procedures employed in M18. However, two aspects are necessarily different. First, the diagnostic Eu lines are either located in the far blue or otherwise weak. This means that the HARPS spectra used by M18, which do not extend below 4800 Å and do not have an extremely high signal-to-noise ratio (S/N), are not suitable. Indeed, M18 could not confidently measure the Eu II $\lambda 6645$ line with an equivalent width (EW) below 10 mÅ in α Cen AB. Second, the Eu II lines are in general strongly blended and broadened by isotopic and hyperfine (HFS) splitting, which calls for an abundance determination relying on spectral synthesis instead of an analysis based on EWs.

For the purpose of this work, our analysis is based on high-resolution HARPS spectra retrieved from the European Southern Observatory (ESO) archives. These have a resolving power, R , of about 115,000 and cover the spectral range 3780–6910 Å. For the solar spectrum to be used as reference, we averaged with a weight that depends on the mean S/N all the available exposures of asteroids with a S/N above 100. Observations of a point-like source are preferred (e.g. Gray et al. 2000), while co-adding spectra from various reflecting bodies is not an issue (e.g. Bedell et al. 2014). For α Cen AB, we collected all spectra with $375 < \text{S/N} < 400$. Spectra with a higher S/N were ignored to avoid saturation problems. For α Cen A, we only considered the numerous spectra obtained over five consecutive nights by Bazot et al. (2007) for their asteroseismic analysis. After rejecting the spectra with Eu features affected by cosmic rays or telluric features (i.e. the molecular lines of the Earth's atmosphere), we ended up with a total of 177, 283, and 284 spectra for the Sun, α Cen A and α Cen B, respectively. However, about 30% of the exposures were discarded for the analysis of Eu II $\lambda 6645$ in α Cen B because of fringing patterns in the red. All spectra were corrected from radial-velocity shifts prior to co-adding based on the precise cross-correlation (CCF) data from the instrument reduction pipeline. The mean spectra were normalised to the continuum by fitting low-order Legendre polynomials using standard tasks implemented in the IRAF⁵ software. To ensure the highest consistency, this procedure was identical for all three stars.

Our results are based on a line-by-line differential analysis relative to the Sun. We make use of plane-parallel, 1D MARCS model atmospheres (Gustafsson et al. 2008) and the 2017 version of the line-analysis software MOOG originally developed by Sneden (1973). M18 carried out the analysis using various line lists taken from the literature. However, only two include Eu features: Meléndez et al. (2014, hereafter Me14) considered Eu II $\lambda 3819.7$, 3907.1, 4129.7 and 6645.1, while the study of Reddy et al. (2003, hereafter Re03) only included Eu II $\lambda 6645.1$. We do not consider Eu II $\lambda 3819.7$ any further because this weak line is

heavily blended and difficult to model properly, as discussed by Lawler et al. (2001). The HFS data are taken from Ivans et al. (2006) and assume the $^{151}\text{Eu}/^{153}\text{Eu}$ isotopic ratio from Chang et al. (1994). The study of Ivans et al. (2006) is an improvement over the reference work of Lawler et al. (2001), as it provides updated Eu transition data. About 30 HFS components are taken into account for each line studied. The lines of other elements in the relevant spectral ranges were modelled using data retrieved from the VALD3 atomic database⁶ and assuming the abundances of M18. For the minor species not included in M18, we scaled the abundances according to [Fe/H] because estimates in the literature are either not robust or for the most part simply not available. We note that this assumption has no impact on our main results. The dissociation energies implemented in MOOG were assumed for the molecular species. To fit the solar spectrum, we adopted projected rotational and macroturbulent velocities of 1.8 and 3.1 km s⁻¹, respectively. For α Cen AB, we assumed the values quoted by Bruntt et al. (2010). Instrumental broadening was also taken into account: the value was first adjusted based on a fit of the relatively unblended Fe II 4128.7 line (see, e.g., Koch & Edvardsson 2002), and then scaled as a function of wavelength according to the full width at half-maximum (FWHM) of lines measured in calibration lamps.

Our strategy was first to adjust the oscillator strengths of lines in vicinity of the Eu feature of interest to optimise the quality of the fit in the Sun. The solar mixture adopted (Grevesse et al. 2007) is consistent with that adopted for the computation of the MARCS model atmospheres. For the solar parameters, we adopted an effective temperature, T_{eff} , of 5777 K, a surface gravity, $\log g$, of 4.44, and a microturbulence, ξ , of 1 km s⁻¹. Finally, to improve the fit in α Cen AB, we altered within their uncertainties the abundances of elements with lines significantly affecting the Eu feature. Similarly to a number of previous studies (e.g. del Peloso et al. 2005; Lawler et al. 2001; Peek 2009), it was occasionally necessary to include in the line list some artificial Fe I lines because of unaccounted absorption. The changes to the initial VALD3 line list are summarised in Table 1. We stress that these slight adjustments lead to a noticeably better fit, but have little impact on the resulting Eu abundances. The modelling of α Cen AB was performed adopting the stellar parameters (T_{eff} , $\log g$ and ξ) derived by M18 for the relevant line list. As for the other elements studied in M18, we used the “unconstrained” results quoted in his table B.2 that are obtained without freezing the surface gravity to the asteroseismic value quoted by Heiter et al. (2015). Illustrative examples of the fits are shown in Fig. 1.

We determine for the Sun an average Eu abundance, $\langle \log \epsilon_{\odot}(\text{Eu}) \rangle = +0.46 \pm 0.05$, based on 1D model atmospheres and assuming local thermodynamic equilibrium (LTE). Theoretical calculations by Mashonkina & Gehren (2000) indicate that the abundances determined from Eu II features must be corrected upwards in solar-like stars to account for departures from LTE. The non-LTE corrections for the Sun amount on average to +0.03 dex for Eu II $\lambda 4429$ and Eu II $\lambda 6645$. On the other hand, 1D-3D corrections appear to be negligible according to CO⁵BOLD hydrodynamical simulations (Mucciarelli et al. 2008). We therefore obtain a corrected solar abundance, $\langle \log \epsilon_{\odot}(\text{Eu}) \rangle = +0.49 \pm 0.05$, that is fully compatible with the recommended meteoritic and photospheric values that lie in the range 0.51–0.52 (Grevesse et al. 2015, and references therein). However, given the differential nature of our analysis with respect to the Sun, we emphasise

⁵ IRAF is distributed by the National Optical Astronomy Observatories, operated by the Association of Universities for Research in Astronomy, Inc., under cooperative agreement with the National Science Foundation.

⁶ <http://vald.astro.uu.se/>

Table 1. Changes made to the initial VALD3 line list. LEP is the lower excitation potential.

Ion	λ (Å)	LEP (eV)	$\log g_f$		Remark
			This study	VALD3	
Eu II λ3907.1					
Fe I	3906.9617	3.283	-2.27	-1.481	$\log g_f$ adjusted
Fe I	3907.22	3.5 ^a	-2.63	...	artificial line
Ce II	3907.2876	1.107	+0.24	+0.320	$\log g_f$ adjusted
Eu II λ4129.7					
Fe I	4129.29	3.5 ^a	-2.95	...	artificial line
Fe I	4129.35	3.5 ^a	-3.1	...	artificial line
Fe I	4129.4600	3.397	-1.89	-1.970	$\log g_f$ adjusted
Fe I	4129.53	3.5 ^a	-3.1	...	artificial line
¹² CN	4129.6006	0.976	-0.8	-0.585	$\log g_f$ adjusted
Ti I	4129.6429	2.239	-1.8	-1.424	$\log g_f$ adjusted
Fe I	4129.956	3.5 ^a	-2.38	...	artificial line
Fe I	4130.0366	1.557	-3.54	-4.034	$\log g_f$ adjusted
Cr I	4130.0614	2.913	-2.6	-0.840	$\log g_f$ adjusted
Eu II λ6645.1					
¹² CN	6644.9153	1.066	-1.825	-2.008	$\log g_f$ adjusted
Si I	6645.2099	6.083	-2.4	-3.156	$\log g_f$ adjusted
Fe I	6645.3645	4.386	-2.95	-3.622	$\log g_f$ adjusted
¹² CN	6645.4038	0.956	-2.087	-1.887	$\log g_f$ adjusted

Notes.

^(a) Arbitrary value adopted following Lawler et al. (2001).

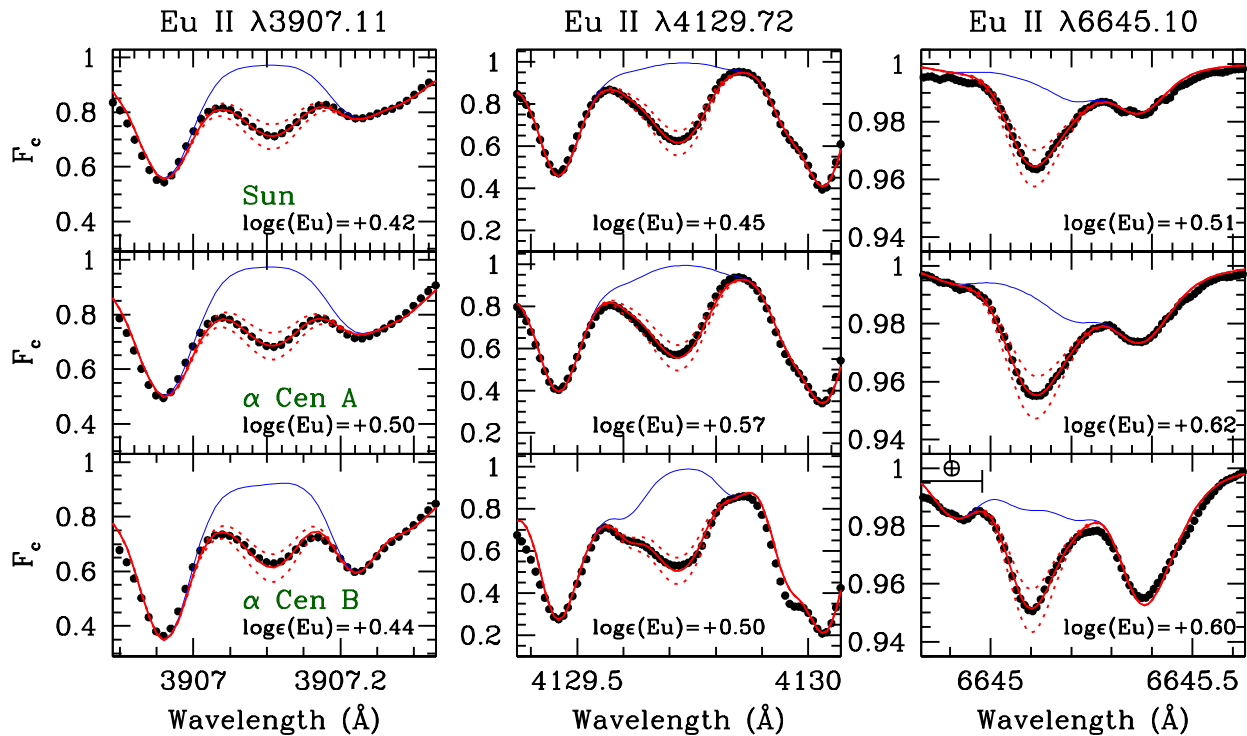


Fig. 1. Examples of fits to the Eu II spectral features in the Sun (top panels) and α Cen AB (middle and bottom panels) based on the line list of Me14. The solid red line shows the best-fitting synthetic profile, while the two dotted lines show the profiles for an Eu abundance deviating by ± 0.1 dex. The blue line shows the profile for no Eu present. The best-fitting abundance is indicated in each case. Note the widely different ordinate scale for Eu II λ 6645. The Earth symbol in the bottom right panel marks the location of telluric features (the Sun and α Cen A are not significantly affected).

that the exact values of the absolute solar abundances have no bearing on our conclusions.

3. Results

The abundance analysis results are summarised in Table 2. Following M18, the random uncertainties are computed by adding

in quadrature the line-to-line scatter, σ_{int} , and the uncertainties arising from errors in the stellar parameters. The larger uncertainties for α Cen B arise from the difficulty in modelling the

Table 2. Abundance results for α Cen AB and comparison to values in the literature. Our recommended values are the weighted average (by the inverse variance) of the results obtained using the Me14 and Re03 line lists. For the analysis based on the single Eu II feature in Re03 line list, we conservatively assumed $\sigma_{\text{int}} = 0.05$ dex.

	[Eu/H]			[Eu/Fe]		
	α Cen A	α Cen B	A–B	α Cen A	α Cen B	A–B
This study						
Me14 line list	+0.10 \pm 0.04 (3)	+0.05 \pm 0.06 (3) ^a	+0.05 \pm 0.07 (3) ^a	-0.12 \pm 0.05 (3)	-0.17 \pm 0.07 (3) ^a	+0.05 \pm 0.08 (3) ^a
Re03 line list	+0.15 \pm 0.06 (1)	+0.16 \pm 0.08 (1) ^a	-0.01 \pm 0.10 (1) ^a	-0.08 \pm 0.07 (1)	-0.07 \pm 0.09 (1) ^a	-0.01 \pm 0.11 (1) ^a
Weighted average	+0.12 \pm 0.04 (3)	+0.09 \pm 0.05 (3) ^a	+0.03 \pm 0.06 (3) ^a	-0.11 \pm 0.04 (3)	-0.14 \pm 0.06 (3) ^a	+0.03 \pm 0.07 (3) ^a
GCE corrected ^b	-0.10 \pm 0.04 (3)	-0.13 \pm 0.06 (3) ^a	+0.03 \pm 0.07 (3) ^a
N97	+0.15 \pm 0.05 (1)	+0.14 \pm 0.05 (1)	+0.01 \pm 0.08 (1)	-0.10 \pm 0.06 (1)	-0.10 \pm 0.06 (1)	+0.00 \pm 0.09 (1)
K02	...	+0.11 \pm 0.08 (1)	-0.08 \pm 0.05 (1)	...
G18	-0.13 \pm 0.14 (3)	-0.03 \pm 0.03 (3)	-0.10 \pm 0.15 (3)

Notes. The number in brackets gives the number of lines used. Keywords for literature studies — N97: Neuforge-Verheecke & Magain (1997); K02: Koch & Edvardsson (2002); G18: Guiglion et al. (2018). Note that the last study made use of archival HARPS spectra that are different from ours. ^(a) These values are affected by a likely underestimation of the abundances in α Cen B at the \sim 0.05 dex level (see Sect. 3). ^(b) Computed from the [Eu/Fe]-age relation of Bedell et al. (2018) (see Sect. 4.1 for details). The uncertainty in the slope of the relation was propagated to the abundances.

spectrum of relatively cool stars exhibiting molecular features and the fact that the stellar parameters are much more sensitive to the choice of the iron line list (see M18).

Tests using Kurucz models indicate that the impact of the choice of the family of 1D model atmospheres is similar for α Cen AB and the Sun, and therefore cancels out to first order through a differential analysis. As discussed in Sect. 2, non-LTE effects in the Sun are very small for Eu II. Although a detailed quantitative investigation is warranted, we thus do not expect differential corrections to significantly bias our results. On the other hand, Mucciarelli et al. (2008) predict negligible 3D corrections for Eu II λ 6645 for stars with parameters representative of those of α Cen AB. The accuracy of our abundance results strongly depends on the reliability of the stellar parameters assumed. For both stars, our T_{eff} is compatible within the uncertainty with the value based on VLTI/PIONIER interferometric measurements (Kervella et al. 2017a). However, the strength of the Eu II lines is particularly sensitive to $\log g$. Although our spectroscopic value for α Cen A is indistinguishable from the accurate asteroseismic estimate, $\log g$ for α Cen B appears to be underestimated by 0.09 and 0.23 dex using Re03 and Me14 line lists, respectively (see M18). We regard this bias as the most significant source of systematic error because it likely leads to an underestimation of [Eu/H] and [Eu/Fe] in this star by \sim 0.05 dex.

4. Discussion

4.1. Comparison with previous results of europium abundances in α Cen AB

Our abundances are in good agreement with previous estimates reported in the literature (Table 2), but our study is generally based on more lines and benefits from higher-quality spectroscopic and HFS data. We do not discuss the results of Allende Prieto et al. (2004) because there is evidence that their T_{eff} scale is too cool (see discussion in M18).

To summarise our abundance analysis results, we find that europium is depleted with respect to iron in α Cen AB by \sim 0.1 dex compared to the Sun and that there is a lack of evidence for a different Eu content in the two components. Our study does not support the claim that the [Eu/Fe] values differ by as much

as 0.16 dex between the two stars (Hinkel & Kane 2013), but we note that Allende Prieto et al. (2004) is their sole literature source for Eu. Our conclusions are still valid if the slight underestimation of the abundances in α Cen B discussed above is taken into account. Generally speaking, we expect the abundances determined through our differential analysis to be more accurate for α Cen A because, in view of the similarity with the solar parameters, they are much less sensitive to deficiencies in the modelling of the atmosphere or non-LTE, 3D and atomic diffusion effects. This caveat affecting the abundances of α Cen B also applies to other differential studies in the literature (e.g. Guiglion et al. 2018).

The exact production sites of europium are still uncertain. Cataclysmic events, such as compact binary mergers or core-collapse supernovae, are proposed to play a role in the nucleosynthesis of Eu, although their relative importance is debated (Skúladóttir et al. 2019, and references therein). The [Eu/Fe] ratios are weakly modulated by Galactic chemical evolution (GCE) effects; the dependence as a function of stellar age appears to be nearly flat (Bedell et al. 2018). Assuming an age for α Cen AB of 6 ± 1 Ga (M18, and references therein) and the linear relations between [Eu/Fe] and age for solar analogues of Bedell et al. (2018), we attribute only \sim 0.01 dex of depletion to GCE (Table 2). Similar GCE effects are also suggested for metal-rich stars (Delgado Mena et al. 2019).

4.2. Comparison of europium abundances between α Cen AB and other FGK stars

In Fig. 2 (*upper panel*), we compare, as a function of [Fe/H], our [Eu/Fe] abundances of α Cen AB to the values for about 570 FGK dwarfs (Delgado Mena et al. 2019). Both α Cen A and B appear on the high and low ends of the [Fe/H] and [Eu/Fe] distributions, respectively, demonstrating their unusual position in the [Fe/H]-[Eu/Fe] locus defined by nearby, thin-disc FGK dwarfs. This conclusion may be sensitive to the (unavoidable) presence of zero-point abundance offsets between our study and Delgado Mena et al. (2019). However, as seen in Fig. 2 (*lower panel*), the same picture holds when considering the separate study of Battistini & Bensby (2016). This indicates that such offsets are unlikely to be much larger than our abundance uncertainties. Hence, the somewhat peculiar position of α Cen AB on

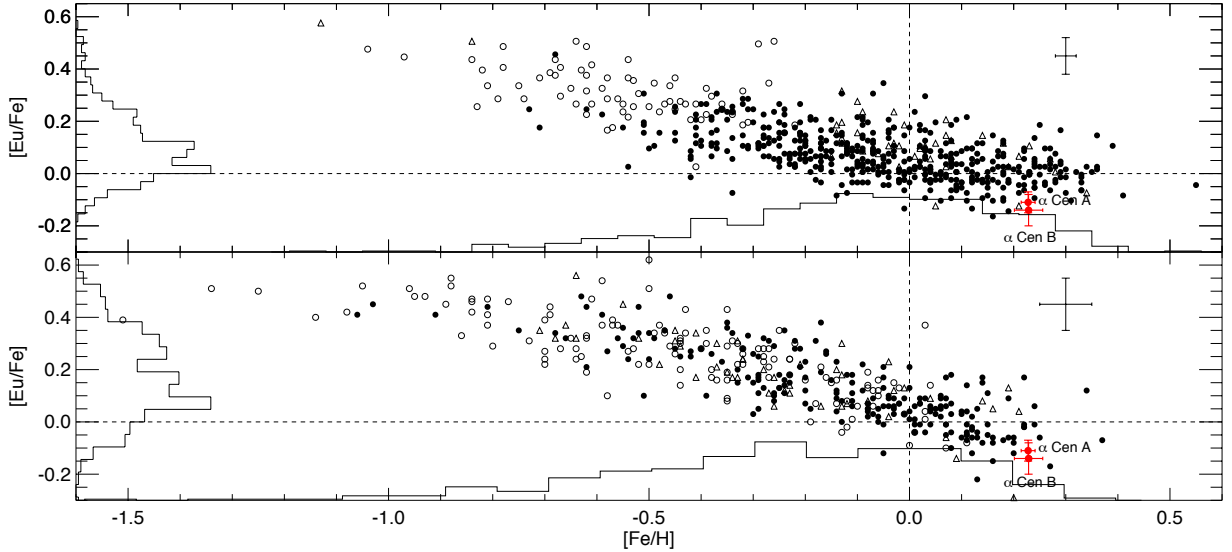


Fig. 2. Our abundance results for α Cen A and B overlain on the [Eu/Fe]-[Fe/H] diagram for large samples of Sun-like stars in the literature. *Upper panel*: data for around 570 FGK stars that have available Eu abundances in Delgado Mena et al. (2017, 2019). The [Eu/Fe] abundances are taken from Delgado Mena et al. (2017), but were shifted upwards by 0.016 dex, as recommended by Delgado Mena et al. (2019). *Lower panel*: same as upper panel, but with data for the 380 FG stars that have available Eu abundances in Battistini & Bensby (2016). The typical uncertainties of the two comparison datasets are shown in the upper right corner of the respective panel. Stars from the thin and thick discs are shown as filled and open circles, respectively, while other stellar populations (i.e. halo, bulge, and uncertain thin-/thick-disc stars) are indicated as open triangles. The histograms on the x-axis and y-axis show the respective distributions of [Fe/H] and [Eu/Fe] of these FG(K) stars. The horizontal and vertical dashed lines indicate the zero points of the diagrams (solar).

the [Fe/H]-[Eu/Fe] locus is most likely a reflection of their true nature.

Using another major rock-forming element than Fe as reference (e.g., Si; Unterborn et al. 2015) would not qualitatively modify our conclusions given that their abundances are tightly correlated with that of iron in thin-disc stars (e.g. Bitsch & Battistini 2020). Indeed, as shown by the [Eu/Si]-[Fe/Si] diagram (Fig. 3), α Cen AB still lie in the lower tail of the [Eu/Si] distribution for the sample of thin-disc stars of Delgado Mena et al. (2019). However, α Cen AB seem to be not a peculiar, but average case, among these comparison stars in terms of [Fe/Si] that alludes to the first-order, planetary internal structure (Wang et al. 2019b).

4.3. Implications for radiogenic heat budgets in putative α-Cen-Earths

To some extent, we can explore implications from the peculiar features of α Cen AB on the distributions of [Eu/Fe] and [Eu/Si] for radiogenic heat production in putative terrestrial-like planets in the system (i.e. "α-Cen-Earth").

First of all, due to the common origin of the binary stars and their overlapped [Eu/Si] and [Fe/Si] abundances (shown in Fig. 3), we do not distinguish such a putative planet around A or B, but compute the weighted average of the Eu abundances in A & B to construct an average α-Cen-Earth of the system.

Second, we need to turn the Eu abundance to the abundances of the *r*-process radioactive elements Th and U (we will discuss K separately). We adopt the observational average (0.014 ± 0.045 dex) of [Th/Eu] values of the solar analogues on the Zero-Age Main Sequence, ZAMS (Botelho et al. 2019) to at first compute Th abundance from Eu. Then the nearly constant $^{238}\text{U}/\text{Th}$ production ratio ($0.571^{+0.037}_{-0.031}$) in meteorites and Galactic halo stars (Dauphas 2005) is adopted to obtain the abundance of ^{238}U . Al-

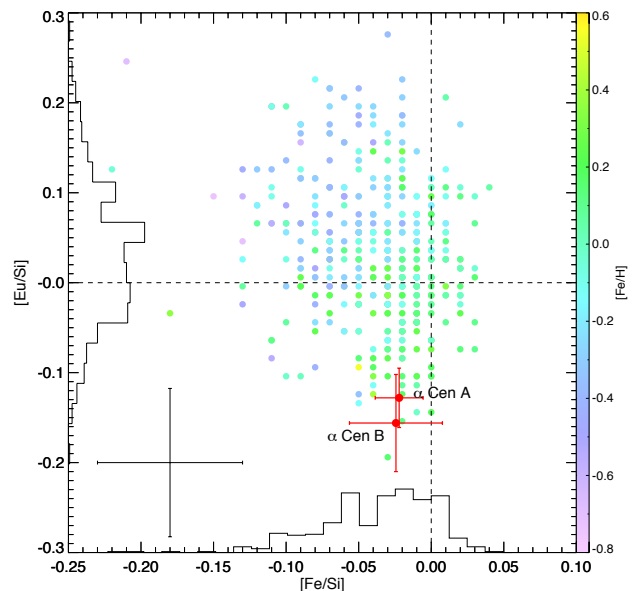


Fig. 3. Our abundance results for α Cen A and B overlain on the [Eu/Si]-[Fe/Si] diagram for the sample of thin-disc stars (colour coded as a function of [Fe/H]) of Delgado Mena et al. (2019). Their typical uncertainties are indicated in the bottom left corner. The histograms on the x-axis and y-axis show the respective distributions of [Fe/Si] and [Eu/Si] of these thin-disc stars. The horizontal and vertical dashed lines indicate the zero points of the diagram (solar).

though the isotopic ratio $^{235}\text{U}/^{238}\text{U}$ may not be necessarily constant during the Galactic history, its variance, however, is limited when considering the time interval between 6 and 9 Ga of the Galactic evolution (Frank et al. 2014); it was within this interval when both the solar system and the α Cen system formed.

Table 3. Model quantities and results of mantle concentrations and heat output of radionuclides in a putative α -Cen-Earth.

Constraint	Value	Reference
$[\text{Eu}/\text{Mg}]^a$	-0.152 ± 0.047	This work & M18
$[\text{Th}/\text{Eu}]^b$	0.014 ± 0.045	Botelho et al. (2019)
$^{238}\text{U}/\text{Th}$	$0.571^{+0.037}_{-0.031}$	Dauphas (2005)
$^{235}\text{U}/^{238}\text{U}^c$	24.286/75.712	Lodders et al. (2009) & Frank et al. (2014)
$M_{\text{Mantle}} (10^{24} \text{ kg})$	4.0312 ± 0.0179	Wang et al. (2018)
Mantle concentration (ppb)		
Nuclide (X)	X/Mg^d	Upon formation ^e
^{232}Th	$1.95^{+0.64}_{-0.48} \times 10^{-7}$	$43.4^{+14.2}_{-10.7}$
^{235}U	$3.61^{+1.2}_{-0.91} \times 10^{-8}$	$8.1^{+2.7}_{-2.0}$
^{238}U	$1.14^{+0.38}_{-0.29} \times 10^{-7}$	$9.7^{+3.3}_{-2.5}$
^{40}K	...	353.6 ± 37.3^g
Heat (TW)		
Nuclide (X)	$h (\text{W/kg})^h$	Upon formation ⁱ
^{232}Th	2.628×10^{-5}	$4.6^{+1.5}_{-1.1}$
^{235}U	5.6847×10^{-4}	$18.5^{+6.2}_{-4.7}$
^{238}U	9.513×10^{-5}	$9.7^{+3.3}_{-2.5}$
^{40}K	2.847×10^{-5}	12.7 ± 1.3
Total	...	$73.4^{+8.3}_{-6.9}$
$8.8^{+1.7}_{-1.3}$		

Notes. ^(a) $[\text{Eu}/\text{Mg}]$ (dex) is calculated from $[\text{Eu}/\text{Fe}] - [\text{Mg}/\text{Fe}]$, where $[\text{Mg}/\text{Fe}]$ comes from the weighted average of the results in M18 obtained using the Me14 and Re03 line lists.

^(b) 100% of Th is ^{232}Th .

^c As explained in text, $^{235}\text{U}/^{238}\text{U}$ refers to the solar system value at the time of its formation (Lodders et al. 2009) based on the limited variance of the ratio within 6–9 Ga into the Galactic history (Frank et al. 2014).

^(d) X/Mg is a mass ratio. While converting differential values (e.g. $^{232}\text{Th}/\text{Mg}$) = $^{232}\text{Th}/\text{Eu}$ - $[\text{Eu}/\text{Mg}]$, in dex) to the mass ratios (e.g. $^{232}\text{Th}/\text{Mg}$) in a linear scale, the reference solar abundances come from Asplund et al. (2009) and the atomic and isotopic masses respectively refer to Wieser et al. (2013) and Audi & Wapstra (1993).

^(e) See text. $C_0(\alpha\text{-Cen-Earth}) = \frac{X/\text{Mg}(\alpha\text{-Cen-Earth})}{X/\text{Mg}(\text{Earth})} \times C_0(\text{Earth})$, where C_0 represents the mantle concentration of an individual radionuclide upon the planet formation; X/Mg (α -Cen-Earth) refers to column 2 in panel 2 of this table (^{40}K is excluded from this calculation); X/Mg (Earth) refers to Table A.1 (for the normalisation purpose, Mg concentration is kept unchanged over geological time).

^(f) See text. $C_t = C_0 \times e^{-t \ln 2/T_{1/2}}$, where t represents the system age (the current age of α Cen AB is 6 ± 1 Ga as of M18); $T_{1/2}$ are the half-lives of these radionuclides (^{232}Th – 14.0 Ga; ^{235}U – 0.704 Ga; ^{238}U – 4.47 Ga; ^{40}K – 1.25 Ga; Turcotte & Schubert 2002).

^(g) See text. Concentration of ^{40}K upon planet formation, $C_0(^{40}\text{K})$, is supplemented by the starting mantle concentration of ^{40}K in the Earth upon its formation, according to the GCE model for cosmochemically Earth-like planets (Frank et al. 2014); the present-day concentration of ^{40}K is calculated through the radioactive decay process following the equation in footnote (f).

^(h) h (the rate of heating per unit mass of a radionuclide) refers to Dye (2012).

⁽ⁱ⁾ Calculated by multiplying the corresponding concentrations (upon planet formation and present day) with the heat generation rates, h , of individual radionuclides.

Hence, we prefer to take a simple approach and adopt the well-known, initial solar system $^{235}\text{U}/^{238}\text{U}$ ratio (24.286/75.712; Lodders et al. 2009), set for 4.56 Ga ago, to infer the abundance of ^{235}U for α Cen AB. We admit that this is a crude simplification, and we discuss this caveat further in the subsequent section.

Third, since both U and Th are refractory lithophile elements (RLEs), their stellar abundances, upon normalising to a major rock-forming RLE (e.g. Mg or Si), implicitly reflect their con-

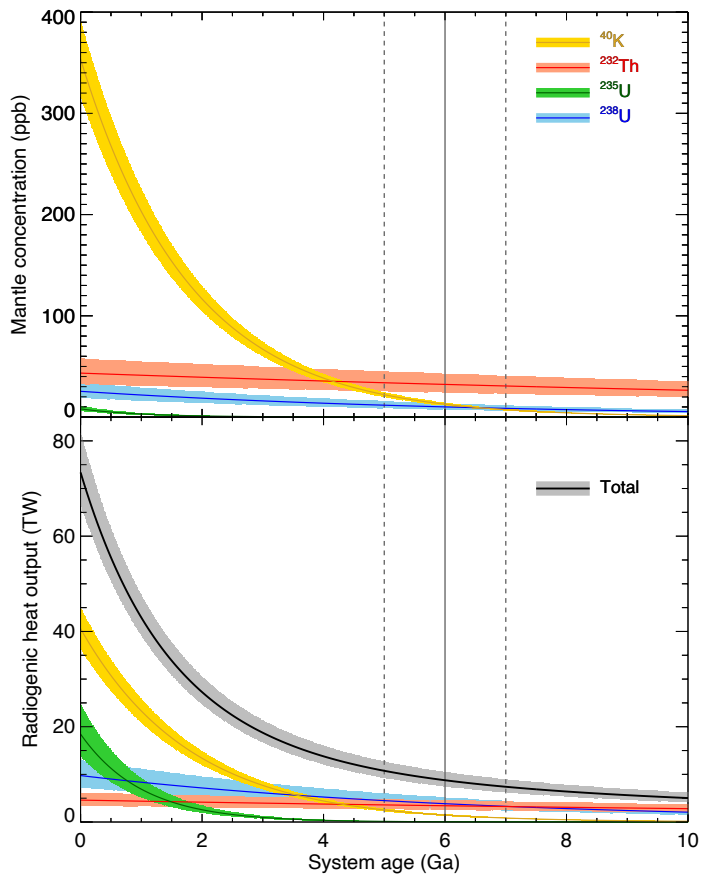


Fig. 4. Estimated mantle concentrations (upper panel) and radiogenic heat output (lower panel) of ^{40}K , ^{232}Th , ^{235}U , and ^{238}U in an α -Cen-Earth as a function of the system age. The wedge around each curve represents the uncertainties of the estimates over the time. The solid and dashed vertical lines indicate the current age (6 ± 1 Ga; Morel 2018) of the α Cen AB system.

centrations in the primitive mantle⁷ of a rocky planet. Here, we prefer Mg over Si because of its more lithophile nature than silicon⁸. On this basis, we can obtain the mass ratio of each individual radionuclide (X) to Mg (i.e. X/Mg). Independently, we can calculate X/Mg of the (primitive) mantle of the Earth based on the literature. With the known mantle concentrations (by mass) of individual radionuclides in the Earth (see Table A.1), we can scale them by the relative X/Mg between α -Cen(-Earth) and the Earth to get the corresponding nuclide concentrations in the primitive mantle of an α -Cen-Earth. For simplicity, the mantle mass of α Cen Earth is assumed to be equal to that of the Earth (this assumption is further discussed in Sect. 4.4).

Furthermore, based on the radioactive decay and their known half-lives (Turcotte & Schubert 2002) as well as the age of the α Cen AB system (6 ± 1 Ga; M18), we model the radionuclide concentrations in the mantle of such an α -Cen-Earth over the geological time. For the normalisation purpose, the concentration of the stable and major-rock forming element Mg in the mantle is kept unchanged.

Eventually, with the heat generation rates (per unit mass of the individual radionuclides; Dye 2012), we compute the heat

⁷ Primitive mantle = present-day mantle + crust.

⁸ Although Si is a lithophile element, it is also widely recognised as a major light element in the core (Wang et al. 2018 and references therein).

output for both the nascent and present-day α -Cen-Earth. We have summarised our model constraints (with references) as well as the concentration and radiogenic heating estimates in Table 3. We have also reported our corresponding calculations for the Earth in Table A.1 for comparison.

Now, we will discuss ^{40}K , which is not directly constrained from Eu but instead, is based on a GCE assumption for cosmochemically Earth-like planets (Frank et al. 2014).

Potassium is not only irrelevant to Eu (in terms of abundances) due to its distinct production and destruction pathways (Clayton 2003; Zhang et al. 2006) but also is a volatile element, which means its abundance in a planet hosting star cannot be directly reflected into a rocky planet (due to devolatilisation during planet formation; Wang 2018, and references therein). Simultaneously, potassium is among a few most challenging (rock-forming) elements to be widely/accurately measured in the photospheres of stars, owing to the fact that only the strong K 7698.96 Å line – that is difficult to model properly and strongly affected by non-LTE effects – is measurable (Reggiani et al. 2019; Takeda 2019) and that it is not covered by most spectrographs (e.g. HARPS). Therefore, at the present time, we are forced to make crude assumptions on the abundance of K or more precisely, ^{40}K . In light of the starting mantle concentrations of ^{40}K ($C^{40}\text{K}$) for cosmochemically Earth-like planets (i.e. assuming their volatile depletion scales relative to their host stars to be the same as that of the Earth to the Sun) as a function of the time after galaxy formation (Frank et al. 2014), we note that the variance in $C^{40}\text{K}$ is insignificant within about 6-9 Ga into the Galactic history. As such, we directly translate the concentration of ^{40}K in the primitive mantle of α -Cen-Earth with that of the primitive mantle of the early Hadean Earth (4.56 Ga ago). For the instantaneous radionuclide concentrations and heat production (due to the radioactive decay), the same processes mentioned earlier will apply (see more details in Table 3 and footnotes therein).

Figure 4 illustrates the calculations of both mantle concentrations and heat output of individual radionuclides (^{232}Th , ^{235}U , ^{238}U , and ^{40}K) in the putative α -Cen-Earth over geological time (logically presumed equal to the system age). In terms of the mantle concentrations, ^{40}K is the most abundant heat-producing nuclide since planet formation until around the age of 4 Ga, when ^{232}Th becomes dominant. ^{238}U is relatively modest over geological time while ^{235}U has become negligible since around 1.5-2 Ga. These trends in concentrations are not exactly identical to those in the heat output of these radionuclides, due to their different heat generation rates. Prominently, ^{235}U contributed a significant amount of heating (only a factor of 2 lower than the highest contributor – ^{40}K) at planet formation and only became negligible since about 4 Ga. ^{238}U has started to play the most significant role in heat production from around the age of 3.5 Ga, when ^{40}K underwent its demise and then was further subordinated by ^{232}Th by the time the system reached 4.5 Ga. Thereafter, ^{238}U and ^{232}Th dominate the radiogenic heat output by contributing approximately equally up to about 10 Ga – the maximum time we have modelled, with ^{232}Th gradually taking over heat production in all old terrestrial-type planets (Frank et al. 2014) owing to its longest half-life (14 Ga).

In comparison with the total radiogenic heat output of the Earth (see Tables 3 and A.1), the α -Cen-Earth generated $73.4^{+8.3}_{-6.9}$ TW at time of formation and $8.8^{+1.7}_{-1.3}$ TW at the present day. We note that this is $23\pm5\%$ and $54\pm5\%$ lower than that estimated for the Hadean Earth (94.9 ± 5.5 TW) and modern Earth (19.0 ± 1.1

TW). In our gedankenexperiment, α -Cen-Earth is intrinsically less geologically active than the Earth, overall.

4.4. Uncertainty/limitation analysis

Our reported uncertainties associated with the radionuclide concentrations and heat output mainly come from the uncertainties on the stellar abundances (Eu and the reference element Mg), those associated with our model constraints, the uncertainties on the mantle concentrations of the Earth, and the uncertainty of the stellar age. The uncertainties of heat output from the individual radionuclides are added in quadrature to estimate the uncertainty of the total heat output. It is noteworthy that uncertainties in a relative sense are smaller than those in absolute values. For example, the comparison of heat output between α -Cen-Earth and the Earth has yielded smaller error bars on their relative differences ($23\pm5\%$ and $54\pm5\%$) than those on the absolute heat output values ($73.4^{+8.3}_{-6.9}$ and $8.8^{+1.7}_{-1.3}$) of α -Cen-Earth, since in the latter case the uncertainties on the reference (the Earth) have also been included.

The accuracy of our model rests on the robustness of our assumptions. We adopted the constant values from Botelho et al. (2019) and Dauphas (2005) for $[\text{Th}/\text{Eu}]$ and $[\text{U}/\text{Th}]$, respectively. We used a constant value for $[\text{Th}/\text{Eu}]$ following Botelho et al. (2019). However, as we noted earlier, the thorium abundance is determined through modelling of a single line that is also heavily blended with other elemental lines, limiting the accuracy of the modelled abundance regardless of the applied treatments. Similar concerns also apply to the U/Th ratio from Dauphas (2005), which may be further affected by the representativeness of the dominant sample of halo stars chosen (even though meteoritic data have also been considered) for the solar-like systems. We emphasize that such measurements/modellings on long-lived radionuclides are, to our knowledge, the best available. For $^{235}\text{U}/^{238}\text{U}$, it may be more appropriate to run GCE corrections on the adopted early solar system value (24.286/75.712; Lodders et al. 2009), in spite of our observation of its limited variance for stars like the Sun and α Cen AB that were formed 6-9 Ga into the Galactic history (Frank et al. 2014). In a more recent work on GCE, Côté et al. (2019) reported an unusually large error bar (60%) on the initial solar system $^{235}\text{U}/^{238}\text{U}$ ratio. If we incorporate it into our calculations, it would have an impact on our reported *error bars* for the starting concentration and heat output of ^{235}U by a factor of about 2, which however is not significant to the total heat output over geological time.

In addition, since we have adopted the concept "cosmochemically Earth-like planets" (Frank et al. 2014) for considering ^{40}K , it limits our conclusions to the total heat budget of habitable-zone terrestrial-like planets. These are supposed to receive the equivalent irradiation from their parent stars as the Earth from the Sun (Hart 1979). Considering that planet formation processes may alter the primordial devolatilisation scale controlled by evaporation/condensation out of a nebular gas (Grossman & Larimer 1974; O'Neill & Palme 2008; Albarède 2009; Hin et al. 2017; Norris & Wood 2017; Wang et al. 2019a; Fegley et al. 2020), such planets might be expected to have shared similar formation histories as our Earth's, at least in terms of the final effect on the volatile depletion. For this reason, we also caution that it is premature to extend our conclusions to the planet(s) orbiting the M5 red dwarf Proxima Cen (Anglada-Escudé et al. 2016; Damasso et al. 2020) in view of the still debated origin of this star (e.g. Kervella et al. 2017b; Beech et al. 2017; Feng & Jones 2018) and the fact that the transposition of the stellar abundances to planet bulk composition might be dramatically

different between Sun-like stars and the chromospherically active, flaring M stars.

Finally, we note that our assumption of the equal mantle mass of a putative α -Cen-Earth as that of the Earth is out of convenience only to enable us to focus on the discussion of the heat output dictated by the estimated mantle concentrations of these radionuclides and then make comparisons between the two planets. It is noteworthy that the current detection limits of radial velocity are still far from being resolvable to any Earth-mass, habitable-zone planet: $M \sin i \sim 50 M_{\oplus}$ for α Cen A and $\sim 8 M_{\oplus}$ for α Cen B (Zhao et al. 2018). On the other hand, the mantle/core ratios between an α -Cen-Earth and the Earth should not be significantly different, in view of the overlapped [Fe/Si] values between α Cen AB and the Sun (Fig. 3). However, we will not go further here in assessing how the planetary mass and mantle/core ratio would affect the radiogenic heat budget; instead, we refer the interested readers to Frank et al. (2014) (in particular, their Sect. 5.2 and Fig. 13) for a detailed discussion of such an aspect.

5. Conclusions

In the context of studying the potential of Eu as a convenient tool to diagnose exoplanetary radiogenic heat power (in the absence of abundance measurements of long-lived radionuclides in the majority of planet hosting stars), we present a detailed determination of the abundances of this element in the photospheres of α Cen AB – our nearest Sun-like stars. Our spectroscopic analysis shows that europium is depleted with respect to iron by ~ 0.1 dex ($\sim 25\%$) and to silicon by ~ 0.15 dex ($\sim 40\%$) compared to solar in both binary components. A comparison with a large sample of FGK stars shows that such a depletion in α Cen AB appears to be true relative to the majority of these Sun-like stars. This may have important implications to the potential of an α -Cen-Earth (a putative terrestrial-like planet in the system) in generating radiogenic heating if our view on using Eu as a proxy for long-lived radionuclides (^{232}Th , ^{235}U and ^{238}U) is correct. ^{40}K has to be treated independently due to its distinct nucleosynthesis pathways and its volatile behaviour.

We have applied a simple and intuitive approach to quantify the radiogenic heat output propagated from the Eu abundances combined with other assumptions including a GCE model for ^{40}K . Our first-order estimates lead us to propose that the radiogenic heat budget in an α -Cen-Earth is $73.4^{+8.3}_{-6.9}$ TW upon its formation and $8.8^{+1.7}_{-1.3}$ TW at the present day, respectively $23 \pm 5\%$ and $54 \pm 5\%$ lower than that in the Hadean Earth (94.9 ± 5.5 TW) and in the modern Earth (19.0 ± 1.1 TW). If we assume all other conditions – especially the primordial gravitational energy (as yet, unconstrained) – are not significantly different between the α -Cen-Earth and our Earth, the mantle convection in the α -Cen-Earth would be comparably weaker than our planet over its equivalent evolution history (as the Earth's), subduing its geological activity and by extension, its long-duration habitable potential.

The multivariate nature of planetary evolution is a complex process (Stevenson 2004), but the similar [Fe/Si] ratios between α Cen AB and the Sun (shown in Fig. 3) reveals to us at the first-order that the relative core-to-mantle mass fractions should not be so different between an α -Cen-Earth and the Earth. Detailed modelling of bulk compositions and internal structures of such α -Cen-Earths will be investigated in our subsequent paper.

In short, we conclude with caution that Eu can be a convenient and practical tool, along with other constraints, in helping understand the exoplanetary radiogenic heating potential. This

may allude to a population analysis of such an aspect for increasingly discovered rocky exoplanets, of which the host stellar abundances for long-lived radionuclides are as yet seldom measurable.

Acknowledgements. We thank D. J. Stevenson for useful comments on an earlier version of the manuscript and C. H. Lineweaver for early discussion. This work has been carried out within the framework of the National Centre of Competence in Research PlanetS supported by the Swiss National Science Foundation. H.S.W and S.P.Q acknowledge the financial support of the SNSF. T.M. acknowledges financial support from Belspo for contract PRODEX PLATO mission development. S.J.M. thanks the Collaborative for Research in Origins (CRIo) at the University of Colorado, which was supported by The John Templeton Foundation (principal investigator: S. Benner/FfAME): the opinions expressed in this publication are those of the authors and do not necessarily reflect the views of the John Templeton Foundation. S.J.M. also acknowledges the NASA Solar System Workings Program, grant No. 80NSSC17K0732 (principle investigator: O. Abramov/PSI). This work has made use of the VALD database, operated at Uppsala University, the Institute of Astronomy RAS in Moscow, and the University of Vienna. This research made use of NASA's Astrophysics Data System Bibliographic Services and the SIMBAD database operated at CDS, Strasbourg (France).

References

Albarède, F. 2009, *Nature*, 461, 1227
 Allende Prieto, C., Barklem, P. S., Lambert, D. L., & Cunha, K. 2004, *A&A*, 420, 183
 Andrade-Ines, E. & Michtchenko, T. A. 2014, *Mon. Not. R. Astron. Soc.*, 444, 2167
 Anglada-Escudé, G., Amado, P. J., Barnes, J., et al. 2016, *Nature*, 536, 437
 Asplund, M., Grevesse, N., Sauval, A. J., & Scott, P. 2009, *Annu. Rev. Astron. Astrophys.*, 47, 481
 Audi, G. & Wapstra, A. 1993, *Nucl. Phys. A*, 565, 1
 Battistini, C. & Bensby, T. 2016, *A&A*, 586, A49
 Bazot, M., Bouchy, F., Kjeldsen, H., et al. 2007, *A&A*, 470, 295
 Bedell, M., Bean, J. L., Meléndez, J., et al. 2018, *ApJ*, 865, 68
 Bedell, M., Meléndez, J., Bean, J. L., et al. 2014, *ApJ*, 795, 23
 Beech, M., McCowan, C., & Peltier, L. 2017, *American Journal of Astronomy and Astrophysics*, 5, 1
 Bisterzo, S., Travaglio, C., Gallino, R., Wiescher, M., & Käppeler, F. 2014, *Astrophys. J.*, 787, 10
 Bisterzo, S., Travaglio, C., Wiescher, M., et al. 2016, *J. Phys. Conf. Ser.*, 665 [arXiv: 1311.5381]
 Bitsch, B. & Battistini, C. 2020, *A&A*, 633, A10
 Bond, J. C., O'Brien, D. P., & Lauretta, D. S. 2010, *ApJ*, 715, 1050
 Botelho, R. B., Milone, A. d. C., Meléndez, J., et al. 2019, *MNRAS*, 482, 1690
 Bruntt, H., Bedding, T. R., Quirion, P.-O., et al. 2010, *MNRAS*, 405, 1907
 Chang, T. L., Qian, Q.-Y., Zhao, M.-T., & Wang, J. 1994, *International Journal of Mass Spectrometry and Ion Processes*, 139, 95
 Clayton, D. D. 2003, *Handbook of isotopes in the cosmos. Hydrogen to gallium* (Cambridge University Press)
 Côté, B., Lugaro, M., Reifarth, R., et al. 2019, *Astrophys. J.*, 878, 156
 Damasso, M., Del Sordo, F., Anglada-Escudé, G., et al. 2020, *Science Advances*, 6, eaax7467
 Dauphas, N. 2005, *Nature*, 435, 1203
 del Peloso, E. F., da Silva, L., & Porto de Mello, G. F. 2005, *A&A*, 434, 275
 Delgado Mena, E., Moya, A., Adibekyan, V., et al. 2019, *A&A*, 624, A78
 Delgado Mena, E., Tsantaki, M., Adibekyan, V. Z., et al. 2017, *A&A*, 606, A94
 Doyle, A. E., Young, E. D., Klein, B., Zuckerman, B., & Schlichting, H. E. 2019, *Science*, 366, 356
 Dumusque, X., Pepe, F., Lovis, C., et al. 2012, *Nature*, 491, 207
 Dye, S. T. 2012, *Rev. Geophys.*, 50, 1
 Fegley, B., Lodders, K., & Jacobson, N. S. 2020, *Chemie der Erde*, 80, 125594
 Feng, F. & Jones, H. R. A. 2018, *MNRAS*, 473, 3185
 Frank, E. a., Meyer, B. S., & Mojzsis, S. J. 2014, *Icarus*, 243, 274
 Gando, a., Gando, Y., Ichimura, K., et al. 2011, *Nat. Geosci.*, 4, 647
 Gray, D. F., Tycner, C., & Brown, K. 2000, *PASP*, 112, 328
 Grevesse, N., Asplund, M., & Sauval, A. J. 2007, *Space Sci. Rev.*, 130, 105
 Grevesse, N., Scott, P., Asplund, M., & Sauval, A. J. 2015, *A&A*, 573, A27
 Grossman, L. & Larimer, J. W. 1974, *Rev. Geophys.*, 12, 71
 Guiglion, G., de Laverny, P., Recio-Blanco, A., & Prantzos, N. 2018, *A&A*, 619, A143
 Gustafsson, B., Edvardsson, B., Eriksson, K., et al. 2008, *A&A*, 486, 951
 Hart, M. H. 1979, *Icarus*, 37, 351
 Hatzes, A. P. 2013, *ApJ*, 770, 133
 Heiter, U., Jofré, P., Gustafsson, B., et al. 2015, *A&A*, 582, A49

Hin, R. C., Coath, C. D., Carter, P. J., et al. 2017, *Nature*, 549, 511

Hinkel, N. R. & Kane, S. R. 2013, *MNRAS*, 432, L36

Hinkel, N. R., Unterborn, C., Kane, S. R., Somers, G., & Galvez, R. 2019, *ApJ*, 880, 49

Hinkel, N. R. & Unterborn, C. T. 2018, *Astrophys. J.*, 853, 83

Ivans, I. I., Simmerer, J., Sneden, C., et al. 2006, *ApJ*, 645, 613

Jacobson, H. R. & Friel, E. D. 2013, *Astron. J.*, 145

Ji, A. P., Frebel, A., Chiti, A., & Simon, J. D. 2016, *Nature*, 531, 610

Kervella, P., Bigot, L., Gallenne, A., & Thévenin, F. 2017a, *A&A*, 597, A137

Kervella, P., Thévenin, F., & Lovis, C. 2017b, *A&A*, 598, L7

Kite, E. S., Manga, M., & Gaidos, E. 2009, *Astrophys. J.*, 700, 1732

Koch, A. & Edvardsson, B. 2002, *A&A*, 381, 500

Korenaga, J. 2008, *Rev. Geophys.*, 46, RG2007

Lawler, J. E., Wickliffe, M. E., den Hartog, E. A., & Sneden, C. 2001, *ApJ*, 563, 1075

Lenardic, A., Cooper, C. M., & Moresi, L. 2011, *Phys. Earth Planet. Inter.*, 188, 127

Lichtenberg, T., Golabek, G. J., Gerya, T. V., & Meyer, M. R. 2016, *Icarus*, 274, 350

Lingam, M. & Loeb, A. 2020, *Astrophys. J.*, 889, L20

Liu, F., Yong, D., Asplund, M., et al. 2020, *Mon. Not. R. Astron. Soc.*, 495, 3961

Lodders, K. 2003, *ApJ*, 591, 1220

Lodders, K., Palme, H., & Gail, H.-P. 2009, in *Landolt-Börnstein, New Ser. Vol. VI/4B*, ed. J. Trümper (Springer-Verlag), 560–598

Lugardo, M., Ott, U., & Keresztszri, Á. 2018, *Progress in Particle and Nuclear Physics*, 102, 1

Lyubetskaya, T. & Korenaga, J. 2007, *J. Geophys. Res. Solid Earth*, 112, 1

Mashonkina, L. & Gehren, T. 2000, *A&A*, 364, 249

Meléndez, J., Ramírez, I., Karakas, A. I., et al. 2014, *ApJ*, 791, 14 (Me14)

Mishenina, T., Kovtyukh, V., Soubiran, C., & Adibekyan, V. Z. 2016, *MNRAS*, 462, 1563

Morel, T. 2018, *A&A*, 615, A172 (M18)

Mucciarelli, A., Caffau, E., Freytag, B., Ludwig, H. G., & Bonifacio, P. 2008, *A&A*, 484, 841

Neuforge-Verheecke, C. & Magain, P. 1997, *A&A*, 328, 261

Nimmo, F. 2015, *Thermal and Compositional Evolution of the Core*, Vol. 9 (Elsevier B.V.), 201–219

Noack, L., Rivoldini, A., & Van Hoolst, T. 2017, *Phys. Earth Planet. Inter.*, 269, 40

Norris, C. A. & Wood, B. J. 2017, *Nature*, 549, 507

O'Neill, H. S. C. & Palme, H. 2008, *Philos. Trans. A. Math. Phys. Eng. Sci.*, 366, 4205

Pagano, M. 2014, Phd thesis, Arizona State University

Pagel, B. E. J. 1989, in *Evolutionary Phenomena in Galaxies*, ed. J. E. Beckman & B. E. J. Pagel, 201

Peek, K. M. G. 2009, *PASP*, 121, 755

Quarles, B. & Lissauer, J. J. 2016, *AJ*, 151, 111

Quarles, B. & Lissauer, J. J. 2018, *AJ*, 155, 130

Rajpaul, V., Aigrain, S., & Roberts, S. 2016, *MNRAS*, 456, L6

Reddy, B. E., Tomkin, J., Lambert, D. L., & Allende Prieto, C. 2003, *MNRAS*, 340, 304 (Re03)

Reggiani, H., Amarsi, A. M., Lind, K., et al. 2019, *Astron. Astrophys.*, 627, 1

Roederer, I. U., Sakari, C. M., Placco, V. M., et al. 2018, *ApJ*, 865, 129

Santos, N. C., Adibekyan, V., Dorn, C., et al. 2017, *Astron. Astrophys.*, 608, 1

Schubert, G., Turcotte, D. L., & Olson, P. 2001, *Mantle Convection in the Earth and Planets* (Cambridge University Press)

Schuler, S. C., Vaz, Z. A., Katime Santrich, O. J., et al. 2015, *ApJ*, 815, 5

Seales, J. & Lenardic, A. 2020, *Astrophys. J.*, 893, 114

Shahar, A., Driscoll, P., Weinberger, Á., & Cody, G. 2019, *Science* (80-.), 364, 433

Simmerer, J., Sneden, C., Cowan, J. J., et al. 2004, *Astrophys. J.*, 617, 1091

Skuladóttir, A., Hansen, C. J., Salvadori, S., & Chopping, A. 2019, *A&A*, 631, A171

Sleep, N. H. 2007, *Treatise Geophys.*, 9, 145

Sneden, C., Cowan, J. J., & Gallino, R. 2008, *Annu. Rev. Astron. Astrophys.*, 46, 241

Sneden, C. A. 1973, PhD thesis, The University of Texas at Austin

Stevenson, D. 2004, *Nature*, 428, 476

Stevenson, D. J. 2003, *Comptes Rendus - Geosci.*, 335, 99

Takeda, Y. 2019, *SAG Stars Galaxies*, 2, id.1

Turcotte, D. L. & Schubert, G. 2002, *Geodynamics* (Cambridge University Press)

Unterborn, C. T., Johnson, J. A., & Panero, W. R. 2015, *Astrophys. J.*, 806, 139

Wang, H. 2018, Phd thesis, Australian National University

Wang, H. S., Lineweaver, C. H., & Ireland, T. R. 2018, *Icarus*, 299, 460

Wang, H. S., Lineweaver, C. H., & Ireland, T. R. 2019a, *Icarus*, 328, 287

Wang, H. S., Liu, F., Ireland, T. R., et al. 2019b, *Mon. Not. R. Astron. Soc.*, 482, 2222

Wieser, M. E., Holden, N., Coplen, T. B., et al. 2013, *Pure Appl. Chem.*, 85, 1047

Wilford, J. 2011, *AUSGEO News*, 101, 8

Wood, B. J., Smythe, D. J., & Harrison, T. 2019, *Am. Mineral.*, 104, 844

Yong, D., Karakas, A. I., Lambert, D. L., Chieffi, A., & Limongi, M. 2008, *Astrophys. J.*, 689, 1031

Zhang, H. W., Gehren, T., Butler, K., Shi, J. R., & Zhao, G. 2006, *Astron. Astrophys.*, 457, 645

Zhao, L., Fischer, D. A., Brewer, J., Giguere, M., & Rojas-Ayala, B. 2018, *AJ*, 155, 24

Appendix A: Radiogenic heat output of the Earth

Table A.1. The estimates of radiogenic heat output in the Earth, respectively upon its formation and present day.

Nuclide (X)	Concentration (ppb)		X/Mg ^c	Heat (TW) ^d	
	Present day ^a	Upon formation ^b		Present day	Upon formation
²³² Th	74.6 ± 6.8	93.5 ± 8.5	4.19 ± 0.38 × 10 ⁻⁷	7.9 ± 0.7	9.9 ± 0.9
²³⁵ U	0.143 ± 0.014	12.7 ± 1.3	5.70 ± 0.58 × 10 ⁻⁸	0.33 ± 0.03	29.1 ± 2.9
²³⁸ U	19.7 ± 2.0	39.9 ± 4.0	1.79 ± 0.18 × 10 ⁻⁷	7.5 ± 0.8	15.3 ± 1.5
⁴⁰ K	28.2 ± 3.0	353.6 ± 37.3	1.59 ± 0.17 × 10 ⁻⁶	3.2 ± 0.3	40.6 ± 4.3
Th+U+K	122.6 ± 7.6	499.6 ± 38.5	...	19.0 ± 1.1	94.9 ± 5.5

Notes. ^(a) Refer to the mantle concentrations of Wang et al. (2018) (column 3 of their Table 1), based on which the radioactive elemental concentrations are converted to the radionuclide concentrations by adopting ²³²Th/Th=1, ²³⁵U/U=0.0072, ²³⁸U/U=0.9928, and ⁴⁰K/K=1.19 × 10⁻⁴ (Turcotte & Schubert 2002) for the present-day bulk silicate Earth.

^(b) $C_0 = C_t \times e^{t \ln 2/T_{1/2}}$, where, C_0 and C_t represent the abundances of a radionuclide upon the Earth formation ($t = 4.56$ Ga) and present day, respectively; $T_{1/2}$ is given in Table 3.

^(c) $X/Mg = C_0(X)/C_0(Mg)$, which refers to the early stage of Hadean Earth (i.e. upon the planet formation); $C_0(Mg) = C(Mg) = 22.3 \pm 0.2\%$ (Wang et al. 2018), i.e., the concentration of Mg is kept unchanged over geological time.

^(d) Calculated by multiplying the corresponding concentrations (upon planet formation and present day) with the heat generation rates, h , of individual radionuclides (see Table 3).